Pressure-enhanced robustness of helical edge state in ABA Tri-layer Graphene

Shijie Fang[1], Hua Fan[2], Jifeng Shao[1,2], Yue Zhao

[1] Shenzhen Institute for Quantum Science and Engineering (SIQSE), Southern University of Science and Technology (SUSTech), China
[2] Department of Physics, Southern University of Science and Technology (SUSTech), China
[3] International Quantum Academy, Shenzhen, Guangdong 518048, China

E-mail: zhaoy@sustech.edu.cn

Abstract

Multi-layer graphene systems are promising platforms to study interesting physical phenomenon, including unique quantum hall physics, spontaneous symmetry breaking and topological properties. Here, by exerting pressure to the tri-layer ABA graphene, we find that the phase diagram at charge neutrality point can have a significant change, indicating a more complex interplay among different energy scales, and the robustness of quantum parity hall state, a kind of helical edge state protected by mirror symmetry, is enhanced. The measured Landau Fan diagram illustrates the modification of the band structure by pressure, which can be used to explain the observed phenomenon.

Keywords: tri-layer ABA graphene, hydrostatic pressure, quantum parity hall effect, exchange interaction

1. Introduction

When it comes to multilayer graphene systems, their rich physical properties make them being widely regarded as a platform to study unconventional properties of two-dimensional electron systems. This perspective has gained broad recognition and has sparked considerable interest among condensed matter physicists. Up to now, numerous research teams have discovered intriguing physical phenomena in multilayer graphene systems, such as Lifshitz transition of Fermi surface topology [1, 2], Landau level crossing in a single particle scenario [3, 4, 5], quantum hall ferromagnetism at high perpendicular magnetic field [6, 7, 8, 9], and various symmetry broken states near charge neutrality and low magnetic field [8,9]. Among them, ABA tri-layer graphene has attracted widespread attention due to its unique band structure at low energy regime. As a highly tunable platform, it provides an excellent opportunity to study its single-particle band structure and many-body phenomenon. In previous studies, researchers have typically analyzed its electronic properties by manipulating carrier density, displacement field, and magnetic field, and have achieved significant results in this system. Notably, due to the highly sensitive low-energy band structure of multilayer graphene, applying pressure to modify the interlayer distance and further study its properties has become a highly promising research approach. Pressure can be viewed as a potent supplement to traditional experimental methods, providing new avenues and experimental schemes for a deeper understanding of physical systems.

In recent years, the field of condensed matter physics has witnessed a growing interest in the exploring the topologically non-trivial edge states in materials. Among them, the helical edge state stands out as a special type of boundary state featuring non-dissipative channels with opposite motion directions. Helical conductors have been proposed by theorists as a platform to realize Majorana statistics for quantum computation[12, 13, 14, 15]. There are multiple ways to achieve helical edge states, including the use of topologically non-trivial band structures protected by time-reversal symmetry, such as those found in QSHE systems [16, 17, 18]. In addition, in systems where the conduction band is energetically below the valence band, the introduction of a magnetic field or displacement field can lead to the intersection of “hole-like” states with “electron-like” states at the system’s boundary, thereby creating a pair of spin-degenerate helical edge states. The advent of multilayer graphene has provided physicists with a versatile platform for exploring different types of helical edge states. This is due to the unique band structure of graphene near the charge neutrality point (CNP) and the high achievable mobility of this material. A wealth of experimental evidence

has confirmed the existence of helical edge states in various graphene configurations, ranging from monolayer to tetralayer graphene [1, 11, 19, 21]. Overall, the exploration of helical edge states and other topological properties has led to exciting advances in condensed matter physics and has potential applications in areas such as quantum information processing and spintronics.

Tri-layer ABA graphene is an interesting material to study quantum hall physics and symmetry-broken states since the low-energy band structure of tri-layer ABA graphene consists of a monolayer-like branch and a bilayer-like branch in the absence of displacement field D, as shown in the Figure1.(b). Both branches are protected by mirror symmetry and have odd and even parity respectively. Although decoupled from each other, the two sets of bands have a noticeable overlap between the monolayer-like valence band and the bilayer-like conduction band, Δ_{mb}. However, when an displacement field is applied, they mix together due to the breaking of mirror symmetry. The unique band structures and symmetries lead to various novel phenomenon, which make the tri-layer ABA graphene interesting.

2. Methods

Here, we fabricate the tri-layer ABA device that has high mobility for observing the clean quantum hall effect in it, and we tune its band structure and quantum phases by exerting hydrostatic pressure out of plane.

Our device is a high-quality dual-gate device with a Hall-bar geometry, which is fabricated by a dry-transfer method [22]. In detail, the tri-layer ABA graphene is encapsulated by two hBN sheets whose geometric capacitances are C_t, C_b in the unit of $V^{-1}\cdot cm^{-2}$. And outside of hBN sheets there are two graphite stacks acting as top gate and bottom gate. By modulating the top gate voltage V_t and bottom-gate voltage V_b, the carrier density $n(10^{12}cm^{-2})$ and out-of-plane displacement field D(V/nm) can be tuned according to the relation : $n = C_tV_t + C_bV_b$, $D = \frac{1}{2\epsilon_0}(C_tV_t - C_bV_b)$, with ϵ_0 the vacuum permittivity. This configuration enables us to do transport measurement with multiple in-situ tunable external parameters.

We also utilize the hydrostatic pressure to reduce the interlayer distance d in order to modify the interlayer coupling strength. Hydrostatic pressure is an excellent way to tune the material structure of multi-layer graphene systems, without enhancing the disorder effect [23,24]. Here we mainly investigate the change of device under a 1.0GP pressure, by comparing it to the that in ambient pressure.

The high quality of this device can be verified by the dependence of longitudinal resistance as a function of $n(10^{12}cm^{-2})$ and $D(V/nm)$. An external out-of-plane displacement field $D(V/nm)$ opens a gap at charge neutrality point which is schematically shown in the Fig.1(b). Fig.1(c) and (d) show the resistance of the device at zero magnetic field before and after pressurization. It is found that, along the charge neutrality point $(n = 0.0 \times 10^{12}cm^{-2})$, the resistance of both increases dramatically when $|D| > 0.1V/nm$, which indicates the appearance of field-induced band gap. This signature reflects a good quality and low disorder of our device before and after pressurization, which enables us to study the sample's band structure using the Landau fan diagram under the application of out-of-plane magnetic field.

In this work, we conducted transport measurements on this tri-layer ABA graphene device before and after pressurization, with n, D, B as variables at temperature T = 1.6K, and our findings are three-fold. Firstly, we explore the phase diagram of the tri-layer ABA graphene at charge neutrality point as a function of magnetic field $B(T)$ and displacement field $D(V/nm)$, by making a slow scan of displacement field D around $0V/nm$ and magnetic field around $B = 0T$. The one after pressurization reveals a complex competition between different energy scales. The interesting thing is that we observe the helical edge state around $D = 0\,V/nm$ after pressurization in magnetic field around $0.5T$, indicated by its quantized four-terminal longitudinal conductance and zero transverse resistance. This state fades away when D is large enough, demonstrating it is protected by mirror symmetry which is broken under finite D.

Secondly, in order to partially explain the observed phenomenon above, we perform the magneto-transport measurement to investigate how the pressure modifies the hopping parameters. Specifically, in the Landau fan diagram, we find that the crossing points among Landau levels undergo a significant shift, appearing at a larger magnetic field at 1.0Gpa pressure. This phenomenon indicates that the strength of interlayer hopping, alternatively the low energy band structure can be modified by pressure.

Finally, in our magneto-transport measurement, we find some signatures of the four-fold quasi-degenerate zeroth monolayer-like Landau levels which can't be explained under the single particle picture. These signatures include the complete splitting of these degenerate Landau levels at relatively high magnetic field $(\sim 10T)$ occurring both before and after pressurization. Besides, we found the Landau level splitting at intermediate magnetic field only after pressurization. These two signatures indicate the enlarged Landau level gaps, which is inconsistent with single particle picture, should be associated with the enhancement of interlayer exchange interaction.

3. Results

3.1 Phase diagram of v=0 at small B

We first investigate the phase diagram of tri-layer ABA graphene around charge neutrality point, by measuring the four-terminal longitudinal conductance G_{xx} (e^2/h) under small

magnetic field and displacement field. The one before and after pressurization are shown in figure 2(a)(b). As can be seen, the phase diagram at 1 Gpa reveals a very different phase diagram than that at 0 Gpa.

Firstly, the phase diagram at 0 Gpa is very similar to that observed in [11]. The conductance around B = 0T and D = 0V/nm is the highest because of the metallic property caused by overlap between valence band and conduction band. As |D| increases, the opening of a band gap at charge neutrality point leads to a quick decrease of G_{xx}, indicating the high quality of our sample. In addition, along the D = 0V/nm profile, a local-minima of G_{xx} emerges around B = 0.25T which is indicated by the green arrows, surrounded by a high-conductance ring. This signature demonstrates that the nature of this state is different from that at higher B or that at zero B. According to [11], a similar state is interpreted as the "Quantum Parity Hall State" (QPH) with quantized four-terminal longitudinal conductance, however, here, we don't observe the well-defined features to claim its edge state configuration, so it can be regarded as an incipient of QPH, and it is not very stable at temperature as high as T = 1.6K whereas the temperature in [11] is 0.4K.

However, at 1 Gpa, the phase diagram becomes very different: the high-conductance state near B = 0T and D = 0V/nm has shrunk into a much smaller region, and more features appear when B and D increase. The first interesting signature is the appearance of spikes of longitudinal conductance G_{xx}(B,D) within a small range of $B \in [0.3T, 0.8T]$, marked by the dashed-line trajectories of different colors in figure 2(b). These signatures refer to the phase boundaries of first order phase transitions, which is accompanied by a sudden change of charge distribution among several flavours [25], driven by the competition between displacement field and magnetic field. Similar experimental results have been found in bilayer graphene and rhombohedral tri-layer graphene, but requires larger magnetic field [26, 27, 28, 29]. We find that one of the phase boundaries display a parabolic-like trajectory at low B (marked by a purple dashed line) and linear trajectory at high B (marked by a green dashed line), whereas another one also displays a linear behaviour (marked by a orange dashed line). These boundaries demonstrate the competition between different energy scales. Based on these phase boundaries and other features, we can divide the phase diagram at charge neutrality point into several regions, and four of them are labelled as A, B, C, D as shown in figure 2(c).

The phase boundary between phase A and phase B could be possibly explained by the competition between exchange interaction caused by B and layer polarization driven by D, since the exchange interaction proportional to $\frac{e^2}{l_B} \sim \sqrt{B}$ whereas the layer polarization characterized by $\Delta_1 = \alpha d D$, with $\alpha \approx 0.3$ the empirical parameters describing the screening effect and $d \approx 0.3nm$ the nearest interlayer distance. Following the analysis of [11], one role of magnetic field is to tune the strength of exchange interaction, whereas the displacement field can cause a layer polarization. So it is reasonable that the competition between phase A and phase B is driven by these energy scales. In contrast, either the phase boundary between phase C and phase B or phase D and phase B, displays a linear-shape trajectory, indicating a different mechanism from that one between phase A and phase B. These linear dependence indicates the energy scale associated with B should also be linear with B. From some theoretical work [6], the Zeeman energy E_{ZM}, difference between intralayer and interlayer exchange interaction δE_{ex} and electrostatic energy E_H are all linear functions of B. Therefore, it is possible that these two phase boundaries appear because of the complex competition between Δ_1 and E_{ZM}, δE_{ex}, E_H.

To better manifest the distribution of electrons in spin and layer flavours, the possible state configurations of phase A/B/C/D are given in the figure 2(c).It is well acknowledged that when D is large enough, the phase would be layer-polarized in order to minimize the ground state energy, mainly driven by the energy scale $\Delta_1 = \alpha e d D$. Therefore the phase C should be fully layer polarized and spin unpolarized. On the other hand, the phase A and phase D should be both spin and layer unpolarized. As discussed below, the phase A holds a non-trivial helical edge state which is spin degenerate. Also, in the absence of displacement field D, the state should have the mirror symmetry which requires zero layer polarization. A interesting problem is what's the configuration of phase B? The appearance of conductance spikes indicate a sudden change of distribution in spin and layer flavours either between phase A/D and phase B or between phase C and phase B. So it is possible that phase B should have some kind of spin polarization. In addition, the slope of boundary between phase B and phase D is almost twice of that between phase B and phase C. This 2:1 ratio may be related to the energy scale associated with the layer coupling. It's possible that the transition between phase A to phase B requires electrons transfer between the two interlayer interfaces (middle layer to top layer and bottom layer to middle layer) whereas the transition between phase C to phase B only requires electrons transfer between one interlayer interface (middle layer to top layer). Based on these, it is possible that the phase B has layer anti-ferromagnetism and is partially layer-polarized, as shown in the figure 2(c).

3.2 Helical edge state protected by mirror symmetry

Next, we find the emergence of the helical edge states after pressurization, which is in the phase A in figure 2(c). To see it clearer, we show the profiles of both four-terminal longitudinal conductance and transverse resistance along the

linecut at D = 0V/nm before and after pressurization in figure.3(a)(b). It can be seen that at 1Gpa, there is a prominent nearly quantized plateau in the longitudinal conductance profile which reaches to about $4\frac{e^2}{h}$(actual $4.1\frac{e^2}{h}$) in a magnetic field ranging from 0.3T to 0.8T, while the transverse resistance drops almost to zero under the same condition. This signature indicates there are two pairs of helical edge states in the phase A.

However, this topological edge state can be destroyed either by increasing B or increasing D. In addition, we extract out the line profiles of Gxx at different B in the range of [0.40T, 0.60T], shown in the figure 3(c). It can be seen that the when the displacement field is large enough, the nearly quantized G_{xx} goes through a drastic increase, indicating the state at D = 0 V/nm is protected by the mirror symmetry. We argue this state is the quantum parity hall state mentioned in [11], which is an analogy to QSHE. The origin of this state can be attributed to the crossing of the zeroth Landau level from the monolayer valence band (m, 0) and the zeroth Landau level from the bilayer conduction band (b, 0) at the sample boundary, forming four spin-degenerate counter-propagating helical edge modes, while the bulk remains insulating, resulting in the quantization of the four-terminal longitudinal conductance G_{xx} to $4e^2$ / h, which can be verified by Landauer-Buttiker formalism. Since the monolayer-like Landau level and bilayer-like Landau level are only valid with the preservation of mirror symmetry, a relatively large displacement field can break this symmetry and hybridize these two types of Landau levels, which leads to the disappearance of the Quantum Parity Hall state.

In addition, the state in [11] exists at temperature 0.4K, whereas the state in our sample is observed at a higher temperature about 1.6K, showing a more robust behaviour against temperature effect. On the other hand, the unstablility of this state before pressurization, indicates that some interlayer hopping parameters may play an important role on the robustness of this state. Indeed, according to [11], the ground state energy of QPH can be expressed as $E_{QPH} = -\frac{15}{4}\sqrt{\frac{\pi}{2}}\frac{e^2}{\epsilon l_B} - 3\Delta_{mb} - \ldots$(... omits other terms), where Δ_{mb} is the energy scale which characterizes the overlap between the valence band of monolayer-branch and the conduction band of bilayer-branch as shown in figure3(d). This expression tells that larger the Δ_{mb}, more stable the QPH state is. To have a more detailed analysis, we have to figure out how the this parameter changes after pressurization in our device. By doing this, we have to figure out how the interlayer hopping parameters are modified after pressurization.

3.3 Extract hopping parameters and estimate interlayer distance

In order to extract the value of hopping parameters, we perform the magneto-transport measurement at these two pressures in the absence of displacement field D, as shown in the figure 4(a) and figure 4(d), which plots the four-terminal longitudinal resistance R_{xx} as a function of carrier density n ($10^{12}cm^{-2}$) and magnetic field B (T). The Landau Fan diagrams can reflect the evolution of Landau levels in tri-layer ABA graphene as the magnetic field changes. At relatively large magnetic field (here 3T), a series of oscillations of broad minima which are separated by broad maxima, emerge with a pattern that each minimum represents the completely filling of one Landau level or several quasi-degenerate Landau levels, depending on the size of Landau level gap. The slope of each minimum track corresponds to a filling factor $\nu = n\frac{h}{eB}$, where e is the electron charge, h is the Planck's constant, and n is the Landau level index. We trace out most of the visible minimum tracks, and plot in figure 4(b) and figure 4(e).

In figure 4(a) and figure 4(d), there are multiple crossing points in each figure with the enhancement of R_{xx} which are caused by the crossing of zeroth Landau levels from monolayer branch (m, 0) and some lowest Landau levels from bilayer branch (b, i) leading to the enhancement of density of states, and we can use the positions of these crossing points to determine the hopping parameters. Some visible crossing points are marked as cyan dot (P_1), red dot (P_2), black dot (P_3) in both figures, which can be identified by (ν, B), and depends on the hopping parameters of tri-layer ABA graphene sensitively. It can be seen that the positions of P_1, P_2, P_3 in Fig.4(b) shift upward to higher fields than that in Fig.4(a), which clearly indicates the modification of hopping parameters after pressurization.

In order to qualitatively explain the modification of hopping parameters, we use the six-band continuum model including all the SWMC parameters (γ_0, γ_1, γ_2, γ_3, γ_4, γ_5, δ, Δ_2), which can be determined by using the positions of crossing points as inputs. The SWMC parameters can be classified as two types: the intra-layer type (γ_0) which are not influenced by inter-layer distance d and the inter-layer type (γ_1, γ_2, γ_3, γ_4, γ_5, δ, Δ_2) which sensitively depends on d so can be modified by quasi-hydrostatic pressure. Here, we determine the positions of P_1, P_2, P_3 as (6, 4.60), (10, 2.40), (14, 1.80) in figure 4(a) and (6, 5.50), (10, 3.00), (14, 2.23) in figure 4(b). Then we optimize the hopping parameters to fit these positions with taking the disorder effect Γ = 0.8meV into account. The fitting results are shown in Table I, and use them to get the simulated Landau level spectra as shown in figure 4(c) and figure 4(f), the positions of Landau levels crossing points (marked by dots of the same colours as in figure 4(a) and figure 4(d)) match well with the experimental result. To explain the enhancement of quantum parity hall effect after pressurization, we find that Δ_{mb} changes several meV after pressurization: it is 14.3meV at 0 Gpa whereas

18.4meV at 1Gpa which has increased about 4 meV after pressurization. This result is consistent with our finding that QPHE is more robust at 1Gpa, since the large Δ_{mb} can help stabilize the ground state energy of Quantum Parity Hall state.

3.4 Features beyond single-particle picture

Within single-particle picture as shown in Fig.4(c) and Fig.4(f), the zeroth Landau levels of monolayer-like branch and some lowest Landau levels of bilayer-like branch are almost degenerate within the valley-spin subspace. With the consideration of disorder effect (Γ = 0.8meV), a set of four-fold Landau levels should be regarded as a four-fold degenerate Landau level, which should reflect in the Landau fan as a single minimum track instead of four splitting minimum tracks. However, the four-fold degeneracy of zeroth Landau level of monolayer-like branch can be lifted off completely at relatively high field both in Fig.4(a) and Fig.4(d), and at even lower field in Fig.4(d). This splitting directly indicates the Landau level gaps becomes larger to make each one isolated with others even with the disorder effect. There are several possible sceneries for this phenomenon : enlarged single-particle gap at large magnetic field, the suppression of disorder effect, and enhanced electron-electron interaction. However, the first two sceneries can be eliminated here with the analysis below. First, the energy of the zeroth Landau levels of monolayer-like branch is constant with K valley $-\frac{\gamma_2}{2}+\Delta_2$ and K' valley $\delta-\frac{\gamma_5}{2}+\Delta_2$, which are not dependent on the magnetic field. This fact eliminates the first one since the Landau level gaps is unchanged. As for the second one, it is also unlikely since the bilayer-like Landau levels doesn't show a clear completely splitting signature at the same magnetic field, even though the gap is larger as shown in the simulation results. In addition, our simulation results show that the zeroth Landau levels of monolayer-like branch are almost degenerate, so even doesn't take the disorder effect into account, the degeneracy shouldn't be totally broken in the single-particle picture. Therefore, this scenario is not possible either. So only the last one, the effect of interaction, can be responsible for it. This phenomenon should be associated with the interaction-induced symmetry-breaking which enlarges the gap further beyond that in the single particle picture. The characteristic energy scale of exchange interaction between Landau levels can be estimated as $E_{ex} = \frac{e^2}{\epsilon l_B} \propto \sqrt{B}$, where $\epsilon \approx 6.6$ is the in-plan h-BN dielectric function. At $B = 10T$, the strength of this interaction can be as large as 27 meV, which is much larger than the single-particle Landau level gaps within the spin-valley subspace. So the electron-electron interaction should not be simply neglected at relatively high field, it can mix all the possible single-particle states together to form new states that spontaneously breaks the symmetry. What's more, the interaction scenario can also be used to explain the splitting happened at a lower field after pressurization. The reduction of interlayer distance d can enhance the inter-layer exchange interaction, which may be important since the monolayer-like branch in tri-layer ABA graphene is layer-coherence. Since the exchange interaction favors symmetry-breaking states, it is possible that the enhancement of inter-layer exchange interaction can help enlarge the gaps even in a relatively lower field [8, 9, 10, 11].

However, there are some doubts that why this enhancement of inter-layer exchange interaction can't enlarge the gaps in bilayer-like branch. Maybe it also relates to the orbital nature of the zeroth Landau level in monolayer-like branch which is only associated with n=0,1 Landau levels. A further study of this phenomenon can be done to reveal the physics behind it, which may be helpful to study the quantum hall ferromagnetism in tri-layer ABA graphene.

4. Conclusion

In conclusion, our work reveals the highly-tunable properties in tri-layer ABA graphene by pressure. It is seen that not only the hopping parameters can be tuned by pressure directly, the phase diagram in the low magnetic field can also have a significant change. These phenomenon demonstrate that tri-layer ABA graphene can be a high-tunable platform for band engineering and a variety of phases with pressurization. It is the emergence of the "Quantum Parity Hall state" which is a helical edge state with 2 pairs of counter propagating edge modes and several novel states favored by different energy scales at charge neutrality point. However, there are still some questions which can't be answered. The first one is about what the nature of the phase B. In order to answer it, it is necessary to use the temperature-varied and tilted magnetic field transport measurement to get a more detailed understanding of the competition between different energy scales. Since the exchange effects and the LL degeneracies are controlled by the perpendicular magnetic field, they may play an important role to determine the phase diagram, revealing the complex Landau level structure of tri-layer ABA graphene. We hope our experimental results can trigger some theoretical and experimental interests to investigate it deeper.

Acknowledgements

Aaa

References

[1] Shi Y, Che S, Zhou K, et al. Tunable Lifshitz transitions and multiband transport in tetralayer graphene[J]. Physical review letters, 2018, 120(9): 096802.Campos L C, Taychatanapat T, Serbyn M, et al. Landau level splittings, phase transitions, and nonuniform charge distribution in trilayer graphene[J]. Physical Review Letters, 2016, 117(6): 066601.

[2] Bao W, Jing L, Velasco Jr J, et al. Stacking-dependent band gap and quantum transport in trilayer graphene[J]. Nature Physics, 2011, 7(12): 948-952.

[3] Taychatanapat T, Watanabe K, Taniguchi T, et al. Quantum Hall effect and Landau-level crossing of Dirac fermions in trilayer graphene[J]. Nature Physics, 2011, 7(8): 621-625.

[4] Campos L C, Taychatanapat T, Serbyn M, et al. Landau level splittings, phase transitions, and nonuniform charge distribution in trilayer graphene[J]. Physical Review Letters, 2016, 117(6): 066601.

[5] Che S, Stepanov P, Ge S, et al. Substrate-Dependent Band Structures in Trilayer Graphene/h− BN Heterostructures[J]. Physical Review Letters, 2020, 125(24): 246401.

[6] Zhang F, Tilahun D, MacDonald A H. Hund's rules for the N= 0 Landau levels of trilayer graphene[J]. Physical Review B, 2012, 85(16): 165139.

[7] Lee Y, Velasco Jr J, Tran D, et al. Broken symmetry quantum Hall states in dual-gated ABA trilayer graphene[J]. Nano letters, 2013, 13(4): 1627-1631.

[8] Stepanov P, Barlas Y, Espiritu T, et al. Tunable symmetries of integer and fractional quantum Hall phases in heterostructures with multiple Dirac bands[J]. Physical review letters, 2016, 117(7): 076807.

[9] Datta B, Dey S, Samanta A, et al. Strong electronic interaction and multiple quantum Hall ferromagnetic phases in trilayer graphene[J]. Nature communications, 2017, 8(1): 14518.

[10] Zibrov A A, Rao P, Kometter C, et al. Emergent Dirac Gullies and Gully-Symmetry-Breaking Quantum Hall States in A B A Trilayer Graphene[J]. Physical Review Letters, 2018, 121(16): 167601.

[11] Stepanov P, Barlas Y, Che S, et al. Quantum parity Hall effect in Bernal-stacked trilayer graphene[J].

[12] Qi X L, Zhang S C. Topological insulators and superconductors[J]. Reviews of Modern Physics, 2011, 83(4): 1057

[13] Hasan M Z, Kane C L. Colloquium: topological insulators[J]. Reviews of modern physics, 2010, 82(4): 3045.

[14] Oreg Y, Refael G, Von Oppen F. Helical liquids and Majorana bound states in quantum wires[J]. Physical review letters, 2010, 105(17): 177002.

[15] Lutchyn R M, Sau J D, Sarma S D. Majorana fermions and a topological phase transition in semiconductor-superconductor heterostructures[J]. Physical review letters, 2010, 105(7): 077001.

[16] Kane C L, Mele E J. Quantum spin Hall effect in graphene[J]. Physical review letters, 2005, 95(22): 226801.

[17] Bernevig B A, Hughes T L, Zhang S C. Quantum spin Hall effect and topological phase transition in HgTe quantum wells[J]. science, 2006, 314(5806): 1757-1761.

[18] Roth A, Brüne C, Buhmann H, et al. Nonlocal transport in the quantum spin Hall state[J]. Science, 2009, 325(5938): 294-297.

[19] Li J, Fu H, Yin Z, et al. Metallic phase and temperature dependence of the ν= 0 quantum hall state in bilayer graphene[J]. Physical review letters, 2019, 122(9): 097701.

[20] Shi Y, Che S, Zhou K, et al. Tunable Lifshitz transitions and multiband transport in tetralayer graphene[J]. Physical review letters, 2018, 120(9): 096802.

[21] Young A F, Sanchez-Yamagishi J D, Hunt B, et al. Tunable symmetry breaking and helical edge transport in a graphene quantum spin Hall state[J]. Nature, 2014, 505(7484): 528-532.

[22] Wang L, Meric I, Huang P Y, et al. One-dimensional electrical contact to a two-dimensional material[J]. Science, 2013, 342(6158): 614-617.

[23] Ke F, Chen Y, Yin K, et al. Large bandgap of pressurized trilayer graphene[J]. Proceedings of the National Academy of Sciences, 2019, 116(19): 9186-9190.

[24] Yankowitz M, Jung J, Laksono E, et al. Dynamic band-structure tuning of graphene moiré superlattices with pressure[J]. Nature, 2018, 557(7705): 404-408.

[25] Zondiner U, Rozen A, Rodan-Legrain D, et al. Cascade of phase transitions and Dirac revivals in magic-angle graphene[J]. Nature, 2020, 582(7811): 203-208.

[26] Geisenhof F R, Winterer F, Seiler A M, et al. Quantum anomalous Hall octet driven by orbital magnetism in bilayer graphene[J]. Nature, 2021, 598(7879): 53-58.

[27] Weitz R T, Allen M T, Feldman B E, et al. Broken-symmetry states in doubly gated suspended bilayer graphene[J]. Science, 2010, 330(6005): 812-816.

[28] Maher P, Dean C R, Young A F, et al. Evidence for a spin phase transition at charge neutrality in bilayer graphene[J]. Nature Physics, 2013, 9(3): 154-158.

[29] Winterer F, Geisenhof F R, Fernandez N, et al. Ferroelectric and anomalous quantum Hall states in bare rhombohedral trilayer graphene[J]. arXiv preprint arXiv:2305.04950, 2023.

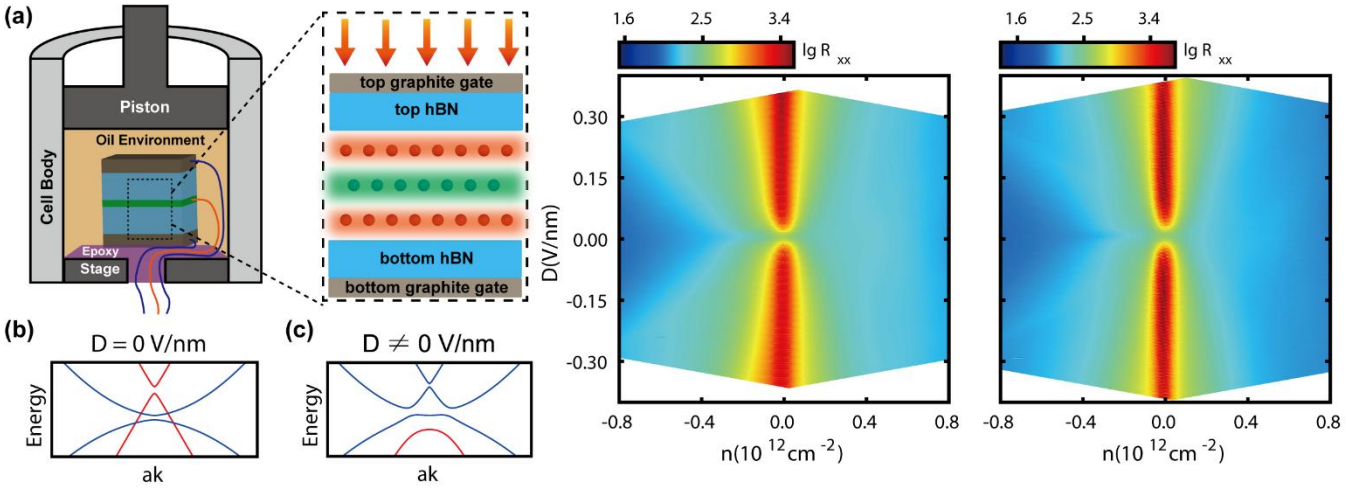

Figure 1 Schematic of experimental setup and transport characterization.

(a) Schematics of hydrostatic pressure setup. (b), (c) Schematics of How the displacement field influence the band structure of tri-layer ABA graphene. When there is no displacement field D, the low energy bands include two monolayer-like bands with linear dispersion (red curve & blue curve), and two bilayer-like bands with parabolic dispersion (cyan curve & green curve). When D is induced, the bands hybridize, opening a gap at charge neutrality point, making it behave insulating. (d), (e) device characterization before and after pressurization by using the four-terminal longitudinal resistance R_{xx} as a function of carrier density n(10^{12} cm^{-2}) and displacement field D(V/nm). Along the charge neutrality profile, it can be seen that as *D* increases, the resistance increases dramatically, indicating a gap opening. These signatures demonstrate the good quality of our device.

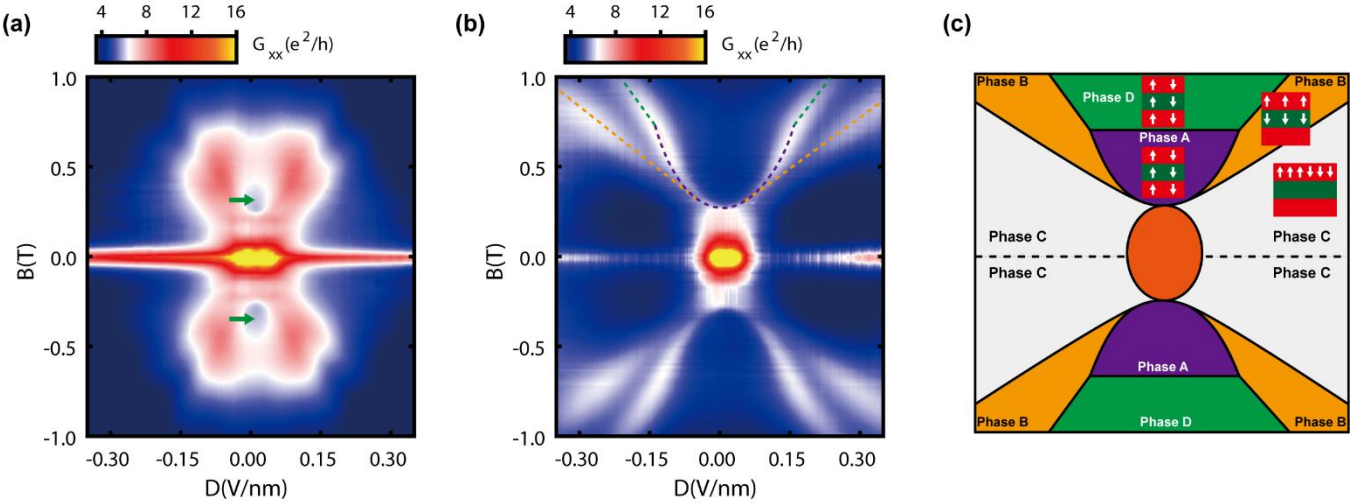

Figure 2 phase diagrams at charge neutrality point before and after pressurization.

Here, we show the phase diagrams of four-terminal longitudinal conductance Gxx in unit of e^2/h as a function of B(T) and D(V/nm), with B ranges from -1.0T to 1.0T and D ranges from -0.30 V/nm to 0.30 V/nm, it is noted that the values larger than 16 has been rescaled to 16. (a) shows the phase diagram at 0 Gpa, a prominent feature of which is a state emerging around D = 0 V/nm and B = 0.3T, indicated by the green arrow. (b) shows the phase diagram at 1GPa with some visible traces of phase boundary (marked by dashed lines of different colors), indicating first-order phase transitions between different ground states. This phase diagram is converted into a schematic image shown in (c), different regions are filled with different colors and specific phases are labelled with A, B, C, indicating different ground states.

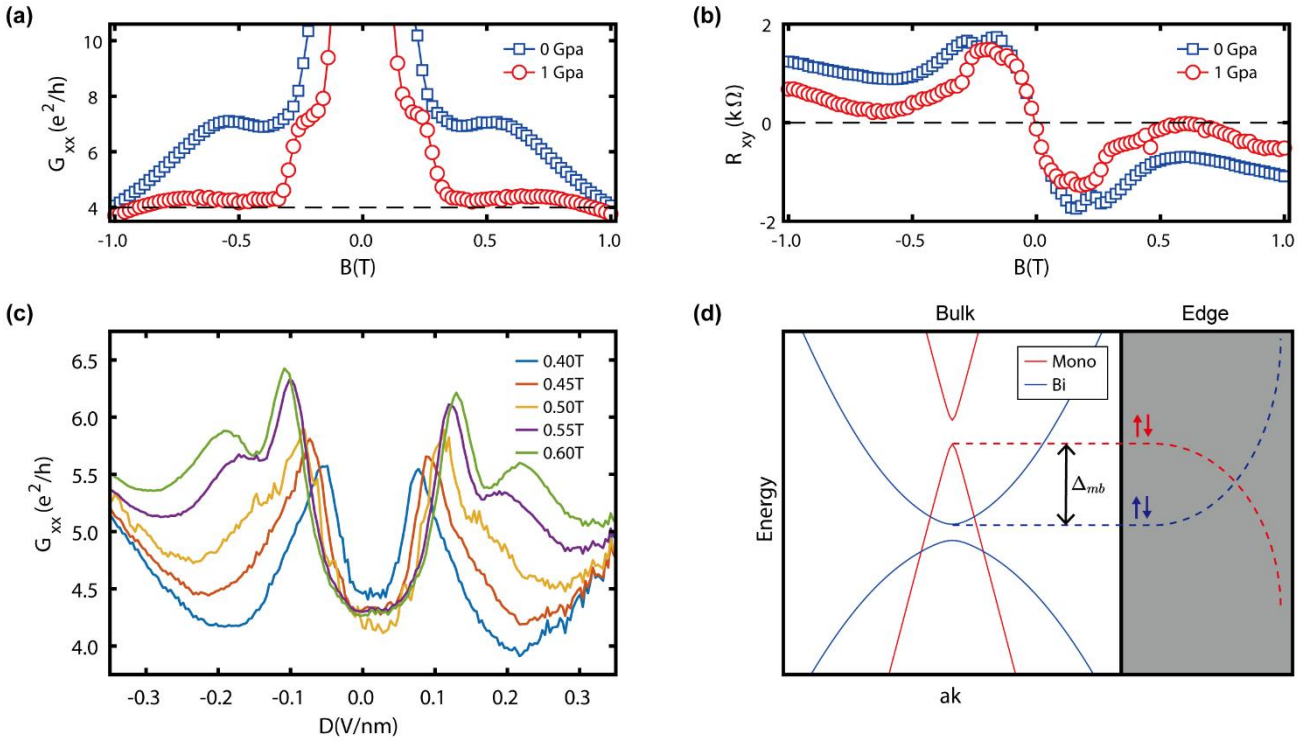

Figure 3 experimental signatures of Quantum Parity Hall effect and its schematics

(a) The longitudinal conductance Gxx profiles of the D = 0 V/nm in both the Figure 2(a) and Figure 2(b), the 0GPa curve is marked by bule squares, and the 1GPa curve is marked by red circles. It can be seen that G_{xx} becomes nearly quantized (about 4.1 e2/h) after pressurization. (b) The profiles of transverse resistance Rxx at D = 0 V/nm, where the 1GPa curve almost reaches to zero around B = 0.6T, together with the nearly quantized signature in (a), indicating appearance of helical edge states in the system, which is called quantum parity hall state (QPHE). (c) The profiles at B = 0.40 / 0.45 / 0.50 / 0.55 / 0.60 T taken from the Figure 2(b), as a function of displacement field D. The nearly quantized plateau disappears when D is large enough. (d) The schematic of the mechanism of (QPHE) based on the band structure : the edge states from monolayer valence band and that from bilayer conduction band propagate along opposite directions along the edge, and because of the spin degeneracy, there are four channels of edge states.

SWMC / Pressure	γ_0	γ_1	γ_2	γ_3	γ_4	γ_5	δ	Δ_2
0GPa	3.100	0.3845	-0.0194	0.3510	0.0653	0.0636	0.0415	0.0021
1.0Gpa	3.100	0.3784	-0.0234	0.3665	0.0612	0.0833	0.0534	0.0031

Table 1 : fitting parameters at 0 Gpa and 1 Gpa based on the experimental results shown in figure.4(a)(b), the energy unit is set to eV. The intralayer hopping γ_0 is fixed as 3.100eV.

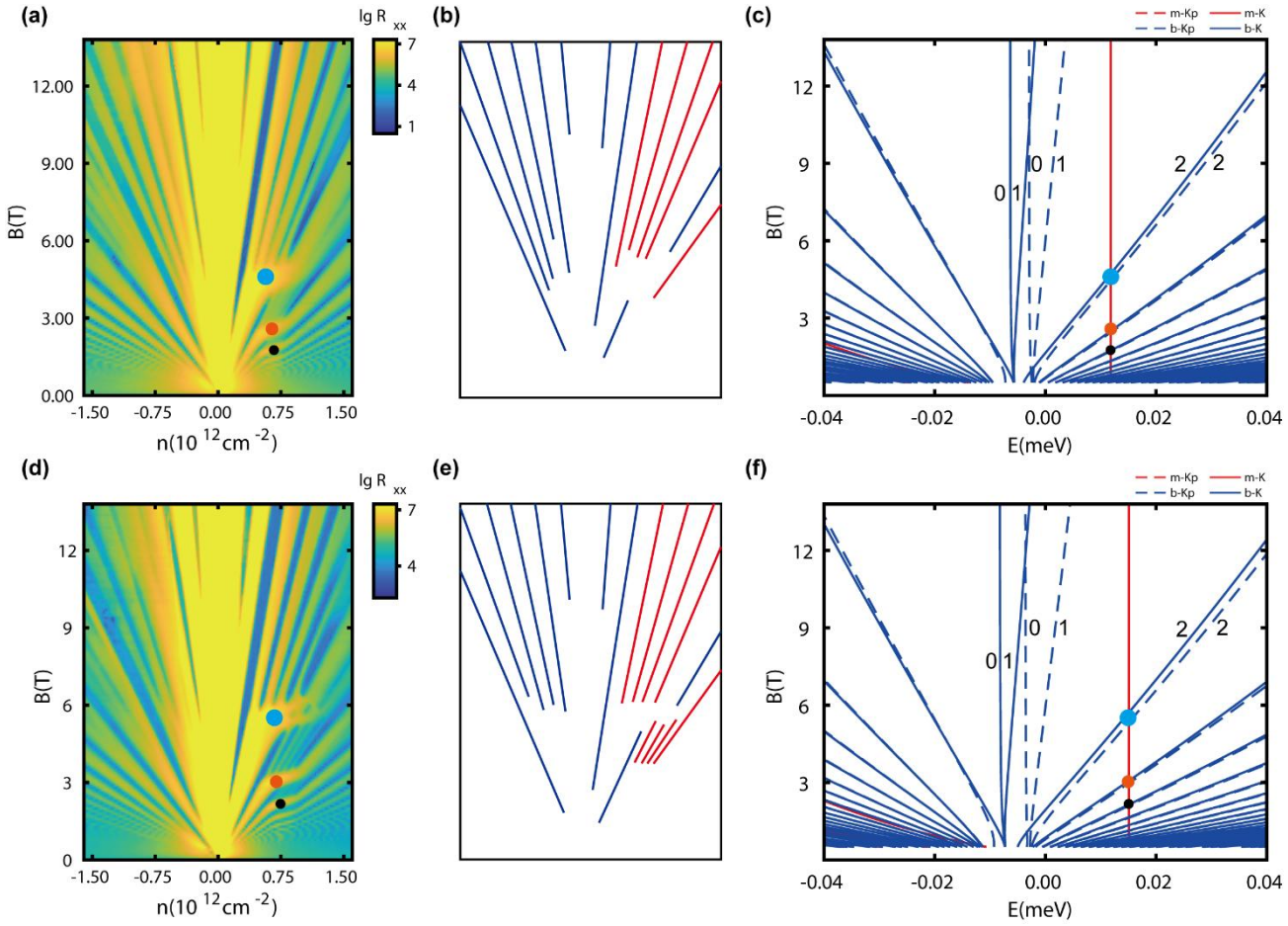

Figure 4 Landau Fan diagrams at 0GPa and 1GPa, and the fitted simulation results.

(a), (d) the Landau Fan diagrams at 0GPa and 1GPa, the crossing points between (m, K/K', 0) and (b, K', 2), (b, K', 3), (b, K', 4) are marked by cyan, orange, black-colored dots (labelled as P_1, P_2, P_3). It can be seen that the crossing points shift toward a large magnetic field after pressurization. In (b), (e), some minimum tracks at low integer fillings (from -6 to 10) are traced out, the blue color indicates that the LLs from bilayer-like branch while the red from monolayer-like branch. (c), (f) the simulated Landau level structures fitted by the positions of crossing points from (a) and (b), the corresponding points are also marked in the figures. The monolayer-like Landau levels are red-color, while the bilayer-like Landau levels are blue-color (dashed line for K' valley and solid line for K valley). The numbers are the Landau level indexes in each branch. The fitting parameters are listed in Table I.